ESTIMATION OF THE DISSIPATION USING PIV IN THE URBAN BOUNDARY LAYER

Karin Blackman

École Centrale de Nantes
LHEEA UMR CNRS 6598
1 Rue de la Noë, 44300 Nantes, France
Karin.Blackman@ec-nantes.fr

Laurent Perret

École Centrale de Nantes
LHEEA UMR CNRS 6598
1 Rue de la Noë, 44300 Nantes, France
Laurent.Perret@ec-nantes.fr

Isabelle Calmet

École Centrale de Nantes
LHEEA UMR CNRS 6598
1 Rue de la Noë, 44300 Nantes, France
Isabelle.Calmet@ec-nantes.fr

ABSTRACT

In the present work a boundary layer developing over a rough-wall consisting of staggered cubes with a plan area packing density $\lambda_p = 25\%$ is studied within the wind tunnel using Particle Image Velocimetry to investigate the Turbulent Kinetic Energy (TKE) budget. An estimation of the dissipation (ε) using both the transport equation of the resolved-scale kinetic energy and a Large-Eddy Particle Image Velocimetry (LE-PIV) model provides the full TKE budget. The presence of the cube roughness elements has a significant influence on the TKE budget due to the strong shear layer that develops over the cubes. The shear layer is shown to produce and dissipate energy, as well as, transport energy through advection, turbulent transport and pressure transport. The recirculation region that forms through interaction of the shear layer and the canopy layer creates rapid longitudinal evolution of the mean flow thereby inducing negative production. Finally, through stochastic estimation of the conditional average it is shown that localized regions of backscatter (energy transfer from unresolved to resolved scales) and forward scatter (energy transfer from resolved to unresolved scales) occur as a result of coherent vortical structures.

INTRODUCTION

Turbulent coherent structures in the lower part of the boundary layer developing over urban terrain are well understood qualitatively, but their quantitative relationships, particularly with regard to energy transfer and production between turbulent structures, are still unknown (Coceal et al., 2007). Due to experimental restraints, very few experimental studies in the urban or rough-wall boundary layer have included significant analysis of the turbulent kinetic energy (TKE or k) budget (Castro et al., 2006).

Typically, experimental methods limit the budget to include only streamwise and vertical velocity components and exclude the direct calculation of the dissipation and pressure transport as normally the spatial resolution of experimental methods is too coarse to resolve the dissipative scales at which the gradients of

$\varepsilon = \frac{1}{2}\nu \overline{\left(\frac{\partial u_i'}{\partial x_j} + \frac{\partial u_j'}{\partial x_i}\right)^2}$ must be calculated (Castro et al., 2006). In previous works the average dissipation has been estimated using analysis of longitudinal velocity spectra (Castro et al., 2006). Other methods for quantifying ε following the Large-Eddy Simulation (LES) formalisation have been proposed including the transport equation of the resolved-scale kinetic energy (Natrajan and Christensen, 2006) and Large-Eddy Particle Image Velocimetry (LE-PIV) based on the use of a sub-grid scale model (Sheng et al., 2000).

Examining the intermittent energy transfer between scales is of specific importance to understanding the flow dynamics and has recently been demonstrated to occur within the smooth-wall boundary layer not only in the direction of large-scales to small-scales (forward scatter), but also from small-scales to larger-scales (backscatter) (Natrajan and Christensen, 2006). Furthermore, this localized regions of forward and backscatter have been linked to the occurence of hairpin vortices. However, this relationship, to the authors' knowledge, has not yet been demonstrated in the rough-wall or urban boundary layer (Natrajan and Christensen, 2006).

The present work aims to use experimental evidence from a boundary layer developing over a staggered cube array to quantify ε and thereby, all the TKE budget terms and to determine which coherent structures are related to the occurrence of backscatter. The quantification of ε will be performed using both the energy transfer equation (Natrajan and Christensen, 2006) and the LE-PIV method proposed by Sheng et al. (2000).

EXPERIMENTAL DETAILS

The experiments were conducted in the low-speed, suction-type boundary layer wind tunnel in the *Laboratoire de recherche en Hydrodynamique, Énergétique et Environnement Atmosphérique* (LHEEA) at École Centrale de Nantes. To initiate the boundary layer development five 800 mm vertical tapered spires were used immediately downstream of the contraction followed by a 200 mm solid fence located 750 mm downstream of the spires. The roughness elements, which consisted of

staggered cubes of height h = 50 mm with a plan area packing density, λ_p, of 25%, then followed. The flow measurements were conducted 19.5 m downstream of the inlet in a vertical plane aligned with the streamwise flow direction. The experiment was performed with a free-stream velocity U_e = 5.8 ms^{-1} measured with a pitot-static tube located 15 m downstream of the inlet at the centre of the wind tunnel, giving a Reynolds number, based on cube height, of Re_h = 1.9x10^4.

The flow measurements were conducted using a Dantec Particle Image Velocimetry (PIV) system set up in stereoscopic configuration to measure all three components of velocity (Figure. 1). A frequency of 5 Hz was used between pairs of pulses of the laser and a time-step of 400 µs was set between two images of the same pair. In total 4000 pairs of images were recorded which corresponds to approximately 9.5 min of measurements. The multi-pass cross-correlation PIV processing resulted in a final interrogation window size of 32 x 32 pixels with an overlap of 50% and a final spatial resolution of 1.7 mm in the streamwise and 2.2 mm in the vertical directions.

RESULTS

Dissipation Estimation

As demonstrated later, the spatial resolution of the present PIV measurements is too coarse to resolve the dissipative scales at which the gradients in the dissipation term ε must be computed. Instead the dissipation was determined using Equation 1 where S_{ij} is the resolved strain rate tensor calculated using Equation 2 and τ_{ij} is the SGS stress tensor.

$$\varepsilon = -\overline{\tau_{ij}S_{ij}} \qquad (1)$$

$$S_{ij} = \frac{1}{2}\left(\frac{\partial \widetilde{U_i}}{\partial x_i} + \frac{\partial \widetilde{U_i}}{\partial x_j}\right) \qquad (2)$$

In these equations $\overline{}$ denotes temporal averaging while $\sim$ denotes spatial filtering. This method is based on the assumption that in high Reynolds number flows TKE is produced by large-scales and cascades to small-scales, which dissipate energy (Sheng et al., 2000). It states that TKE is produced by the integral scales while energy is dissipated by the Kolmogorov scales at the same rate that it is produced, thus within the inertial subrange TKE is neither produced nor dissipated and these structures simply transfer energy from large to small-scales without changing (Sheng et al., 2000). Therefore, the turbulent dissipation is equal to the energy transfer in the inertial range.

To compute τ_{ij} we follow the LES formalism, which uses spatial filtering resulting in scale separation. In this formalism τ_{ij} is defined as Equation 3.

$$\tau_{ij_{ET}} = \widetilde{u_i u_j} - \widetilde{u_i}\widetilde{u_j} \qquad (3)$$

This method is referred to as the direct energy transfer method and directly calculates the energy transfer between the large-scale filtered turbulence and the small-scale structures (Natrajan and Christensen, 2006). Due to the low spatial resolution of the PIV the small-scale structures in the flow are not fully captured, thus, this method may neglect small-scale structures important to dissipation.

A second method which uses a subgrid scale model, as in LES computations, is used and referred to as the LE-PIV method (Sheng et al., 2000). In the present work the gradient model as outlined by Clark et al. (1979) is used to estimate ε of the SGS (Equation 4).

$$\tau_{ij_{LE-PIV}} = \frac{1}{12}\Delta^2 \left(\frac{\partial \widetilde{U_i}}{\partial x_k}\right)\left(\frac{\partial \widetilde{U_j}}{\partial x_k}\right) \qquad (4)$$

In this equation Δ denotes the size of the spatial filter used.

In the present work the measurements were performed in one plane only making it impossible to compute all of the necessary gradients. Instead the missing gradients are computed using the divergence-free condition and an assumption of isotropy.

Estimation of the dissipation using these two methods requires special treatment of the data. A low-pass filter must be applied to the data prior to the computation of the velocity gradients, using a cut-off wavelength larger than the Taylor micro-scale (λ) to ensure a clear cut-off within the inertial range where the equivalence between the scale energy transfer and the dissipation holds (Sheng et al., 2000).

To determine the cut-off wavelength required for the low-pass filter the dissipation was estimated using both the LE-PIV and the energy transfer method with different low-pass filter sizes applied (not shown). The dissipation estimate is independent of the filter cut-off wavelength if this parameter lies in the inertial range of the turbulent energy spectrum. Using this criteria in the present work at heights z/h < 0.8 a filter of size $\Delta_1(x, z) = (0.58h, 0.13h)$ is applied while at heights z/h ≥ 0.8 a filter of size $\Delta_2(x, z) = (0.44h, 0.13h)$ is sufficient. In addition, the Taylor microscale λ is estimated using Equation 5 and compared with the low-pass filter size to ensure that the chosen cut-off wavelength is larger than λ (not shown).

$$\lambda = \left(15\overline{u'^2}\,\nu \big/ \varepsilon_{LE-PIV}\right)^{1/2} \qquad (5)$$

Figure 2 shows ε calculated using both the LE-PIV method and the direct energy transfer method at B from Figure 1. At this location, the two estimations agree well, to within 10%, however, close to the upstream cube (not shown), there is a significant discrepancy, up to 40%, between the two models within the shear layer and the canopy. This large discrepancy is a result of the low PIV spatial resolution neglecting small-scale structures important to the dissipation in the wake of the cube. Those structures are not taken into account by the direct energy transfer method, but their influence is modelled by the LE-PIV model, therefore, the LE-PIV model will be used in the remaining analysis of the present work.

Turbulent Kinetic Energy Budget
The general form of the TKE budget for a stationary flow is described in Equation 6, where *Adv* is advection, *P* is production, *T* is turbulent transport, Ψ is pressure transport, *D* is viscous transport and ε is dissipation. In the present work Adv, P and T are calculated directly from the PIV measurements, ε is estimated using the methods described above, *D* is considered negligible for high Reynolds number flows and finally, Ψ is estimated as the residual of the budget.

$$0 = \underbrace{-\overline{u}_j \frac{\partial \overline{k}}{\partial x_j}}_{Adv} \quad \underbrace{-\overline{u_i' u_j'} \frac{\partial \overline{u}_i}{\partial x_j}}_{P} \quad \underbrace{-\frac{1}{2} \frac{\partial \overline{u_i' u_i' u_j'}}{\partial x_j}}_{T}$$

$$\underbrace{-\frac{1}{\rho} \frac{\partial \overline{P' u_j'}}{\partial x_j}}_{\Psi} + \underbrace{\nu \frac{\partial}{\partial x_j} \left[\overline{u_i' \left(\frac{\partial u_i'}{\partial x_j} + \frac{\partial u_j'}{\partial x_i} \right)} \right]}_{D} - \epsilon \qquad (6)$$

Figure 3 shows the TKE budget at A, B and C behind a cube obstacle. The production of energy is balanced by the dissipation above the height of z/h > 2, while all other terms are negligible. Close to the obstacles (Figure 3a), the strong shear layer induced by the presence of the roughness elements causes energy production, which decreases in magnitude as the shear layer develops over the canopy (Figure 3c). There is also dissipation of energy within the shear layer and transportation of energy by the shear layer to the canopy and overlying boundary layer through advection, turbulent transport and pressure. Finally, pressure transport is balanced by production and turbulent transport within the canopy where it is an energy sink (Figure 3b,c) except close to the upstream cube where pressure transport becomes an energy source (Figure 3a). This region, which contains a recirculation region, also exhibits high magnitudes of dissipation and negative production.

The variation of production with x/h, specifically the negative production close to the upstream roughness, requires further examination. The production decomposed into the contribution of each velocity gradient term at A and B is shown in Figure 4. The term $-\overline{u'w'}\,\partial\overline{U}/\partial z$ is the largest contributor at both locations, which is a result of the strong shear layer that is induced by the presence of the roughness. However, within the canopy close to the upstream cube there is a large contribution of the term $-\overline{u'u'}\,\partial\overline{U}/\partial x$ which causes negative production in this region (Figure 4a). Negative production suggests flow is not in equilibrium and it has been previously shown to occur in asymmetric flows such as, around a wall-mounted cube (Yakhot et al., 2006). It is attributed to a rapid change of the flow in the recirculation region, resulting in positive $\partial\overline{U}/\partial x$ (Yakhot et al., 2006). In the present work a rapid increase occurs within the wake of the upstream cube at A (Figure 4c) where the shear layer interacts with the canopy layer forming a recirculation region with large positive $\partial\overline{U}/\partial x$. Downstream of the wake the term $-\overline{u'u'}\,\partial\overline{U}/\partial x$ becomes positive reaching a maximum just above the canopy layer suggesting that in this region this term is related to the growth of the shear layer.

Backscatter and coherent structures

As mentioned above, recent work has demonstrated that instantaneous dissipation occurs not only in the direction of large-scales to small-scales (forward scatter), but also from small-scales to larger-scales (backscatter) (Natrajan and Christensen, 2006). Within the overlying boundary layer backscatter events have been linked to coherent hairpin vortices which have been shown to be qualitatively similar to those found in the rough-wall boundary layer (Carper and Porté-Agel, 2004; Natrajan and Christensen,

2006). Conditional averages will be used to determine the nature of the flow structures related to these backscatter events in the present rough-wall boundary layer.

A threshold is imposed at each grid location to ensure only significant forward scatter (ϵ_f) and backscatter (ϵ_b) events are included in this analysis thereby minimizing any decorrelation caused by weak or insignificant dissipation events (Natrajan and Christensen, 2006). The threshold used in the present work is based on the mean forward scatter (ε^+) and backscatter (ε^-) at each grid location, which corresponds to the threshold applied by Natrajan and Christensen (2006) in the smooth-wall boundary layer. Thus, the instantaneous dissipation at each grid location is

$$\phi(x,y) = \begin{cases} \epsilon_f = \epsilon & \text{if } \epsilon > \varepsilon^+ \\ \epsilon_b = \epsilon & \text{if } \epsilon < \varepsilon^- \\ 0 & \text{otherwise} \end{cases} \qquad (7)$$

Conditional averages are used to determine whether these instantaneous forward and backscatter events occur consistently with individual vortical structures in the boundary layer. Due to the large number of events that must be included for statistical convergence direct computation of the conditional average is not possible, instead Stochastic Estimation (SE) will be used to estimate the conditional average (Adrian, 1975). SE estimates the conditional average from unconditional correlations by minimizing the mean-square error between the true conditional average and a given estimate. The conditional average of the forward scatter or backscatter event associated with a vortical structure is therefore,

$$\overline{\phi(x,y)|\lambda_{ci}(x_r,y_r)} = \frac{\overline{\phi(x,y,z)\lambda_{ci}(x_r,y_r)}}{\overline{\lambda_{ci}(x_r,y_r)\lambda_{ci}(x_r,y_r)}} \lambda_{ci}(x_r,y_r) \qquad (8)$$

where (x_r, y_r) is the chosen reference location and λ_{ci} is the swirling strength, which is the imaginary part of the complex eigenvalues of the velocity gradient tensor.

The average velocity field associated with the swirling event can also be estimated as

$$\overline{u'_j(x,y)|\lambda_{ci}(x_r,y_r)} = \frac{\overline{u'_j(x,y,z)\lambda_{ci}(x_r,y_r)}}{\overline{\lambda_{ci}(x_r,y_r)\lambda_{ci}(x_r,y_r)}} \lambda_{ci}(x_r,y_r) \qquad (9)$$

where u'_j is the jth fluctuating velocity component.

Figure 5 shows the conditionally averaged forward and back scatter contours along with the streamwise and vertical velocity fluctuations associated with a swirling event at z/h = 1 within the shear layer and z/h = 4 within the boundary layer. To improve the estimate the conditional average was computed using a reference location (x_r) at each x/h grid location and then spatially averaged in the x-direction so that $\delta x = x - x_r$. Within the shear layer the small-scale vortical structures contribute directly to both strong forward and backscatter in this region (Figure 5a,b). The forward and backscatter occur in front of and behind the swirling event due to the shape of the shear layer. However, within the boundary layer localized peaks of forward scatter are shown to occur in front of and behind the swirling event, while strong backscatter occurs above and upstream of the swirling event and below and downstream of the vortex core (Figure 5c,d). This agrees with results from the smooth-wall boundary layer, which linked these forward and backscatter events to coherent hairpin vortices (Carper and Porté-Agel, 2004; Natrajan and Christensen, 2006). In the present work the presence of the roughness elements induces a strong shear layer containing small-scale structures that produce both strong forward and backscatter resulting in two distinct flow regions with distinct relationships to the dissipation of energy.

CONCLUSIONS

In the present work experimental evidence from an urban-type boundary layer consisting of a staggered cube array was used to analyze the Turbulent Kinetic Energy Budget and the following conclusions found.

Two methods were used to estimate ε, an LE-PIV gradient model (Sheng et al., 2000) and a direct energy transfer calculation (Natrajan and Christensen, 2006). To ensure that the separation between the large-scales and the small-scales occurs within the inertial range of the velocity spectra both methods estimate ε using a low-pass spatial filter with a cut-off wavelength larger than the Taylor microscale (Sheng et al., 2000). The other budget terms were calculated directly from the PIV measurements with pressure transport as the residual of the budget.

The budget terms were found to be significantly influenced by the presence of the roughness elements, which induces a strong shear layer. The shear layer is shown to produce and dissipate energy, as well as, transport energy through advection, turbulent transport and pressure transport. The magnitudes of the production and dissipation of energy decrease as the shear layer develops over the canopy. Within the wake of the upstream cube a recirculation region is formed through interaction of the shear layer and the canopy layer which creates positive pressure transport. This region also contains small-scales structures that dissipate energy. Furthermore, the recirculation region results in a rapid increase of the streamwise velocity component in the longitudinal direction thereby generating negative production.

Finally, through stochastic estimation of the conditional average it was shown, similar to the smooth-wall boundary layer, that localized regions of forward scatter occur in front of and behind a hairpin head, whereas, backscatter occurs above and upstream and below and downstream of a hairpin head. However, the presence of the roughness elements induces a strong shear layer that contains small-scale vortical structures that contribute significantly to both forward and backscatter events within the shear layer.

REFERENCES

Adrian, R. J., 1975, "On the role of conditional averages in turbulence theory," *Proceedings, 4th Biennial Symposium Turbulence in Liquids*, Princeton, N.J., Science Press, Rolla, Missouri, pp. 323-332.

Carper, M.A., Porté-Agel, F., 2004, "The role of coherent structures in subfilter-scale dissipation of turbulence measured in the atmospheric surface layer", *Journal of Turbulence*, Vol. 5, pp. 40-64.

Castro, I.P., Cheng, H., Reynolds, R., 2006, "Turbulence over urban-type roughness: deductions from wind-tunnel measurements", *Boundary Layer Meteorology*, Vol. 118, pp. 109-131.

Coceal, O., Dobre, A., Thomas, T.G., 2007, "Unsteady dynamics and organized structures from DNS over an idealized building canopy", *International Journal of Climatology*, Vol. 27, pp. 1943-1953.

Natrajan, V.K., Christensen, K.T., 2006, "The role of coherent structures in subgrid-scale energy transfer within the log layer of wall turbulence", *Physics of Fluids*, Vol. 18, pp. 065104.

Sheng, J., Meng, H., Fox, R.O., 2000, "A large eddy PIV method for turbulence dissipation rate estimation", *Chemical Engineering Science*, Vol. 55, pp. 4423-4434.

Yakhot, A., Liu, H., Nikitin, N., 2006, "Turbulent flow around a wall-mounted cube: A direct numerical simulation", *International Journal of Heat and Fluid Flow*, Vol. 27, pp. 994-1009.

ACKNOWLEDGMENTS
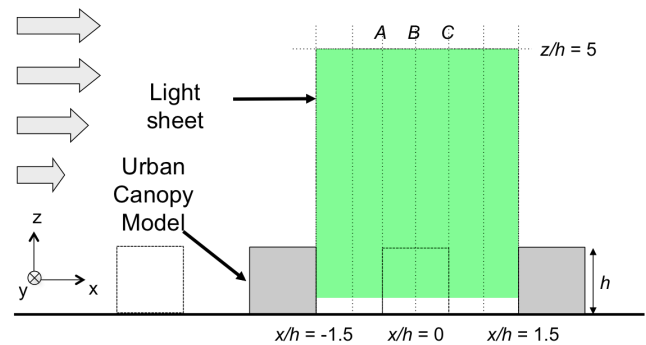
Figure 1. Wind tunnel stereoscopic PIV set-up with PIV measurement region (—) in the x-z plane.
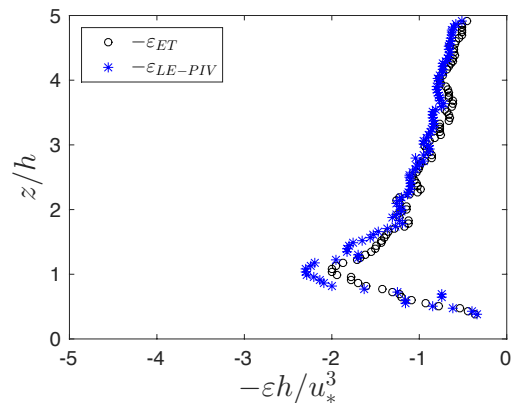
Figure 2. Mean dissipation at *B* calculated using direct energy transfer, ET (o) and LE-PIV gradient model (*) with all terms normalized by h/u_*^3.

a)

b)

c)
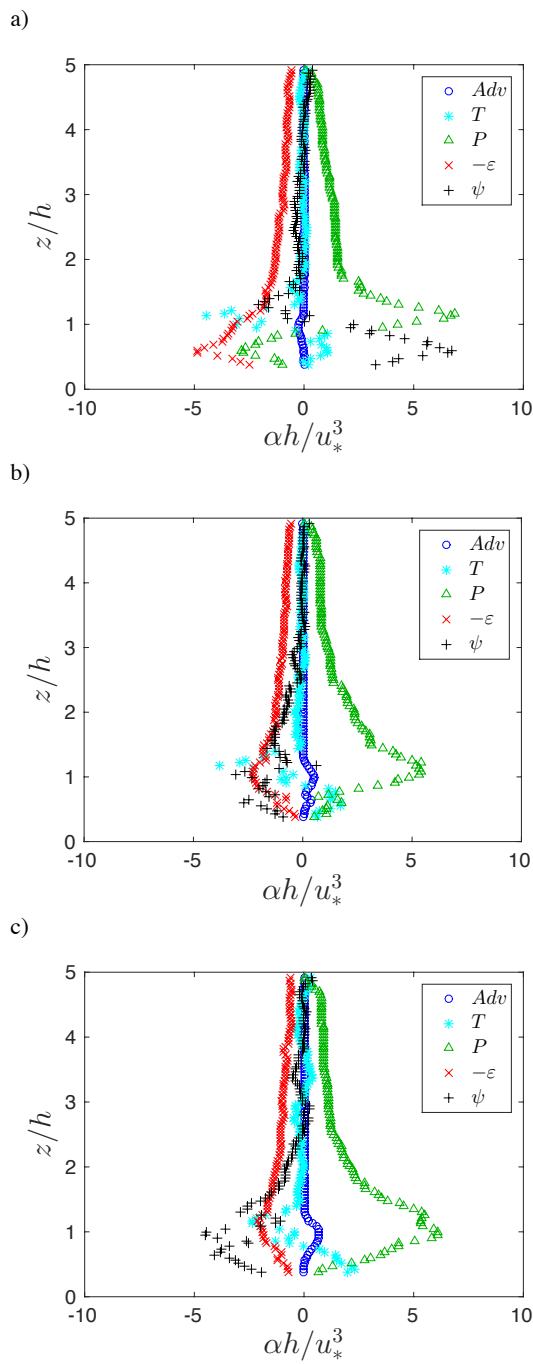
Figure 3. Turbulent Kinetic Energy Budget with ε_{LE-PIV} dissipation at a) A; b) B; c) C with all terms normalized by h/u_*^3.

a)

b)

c)
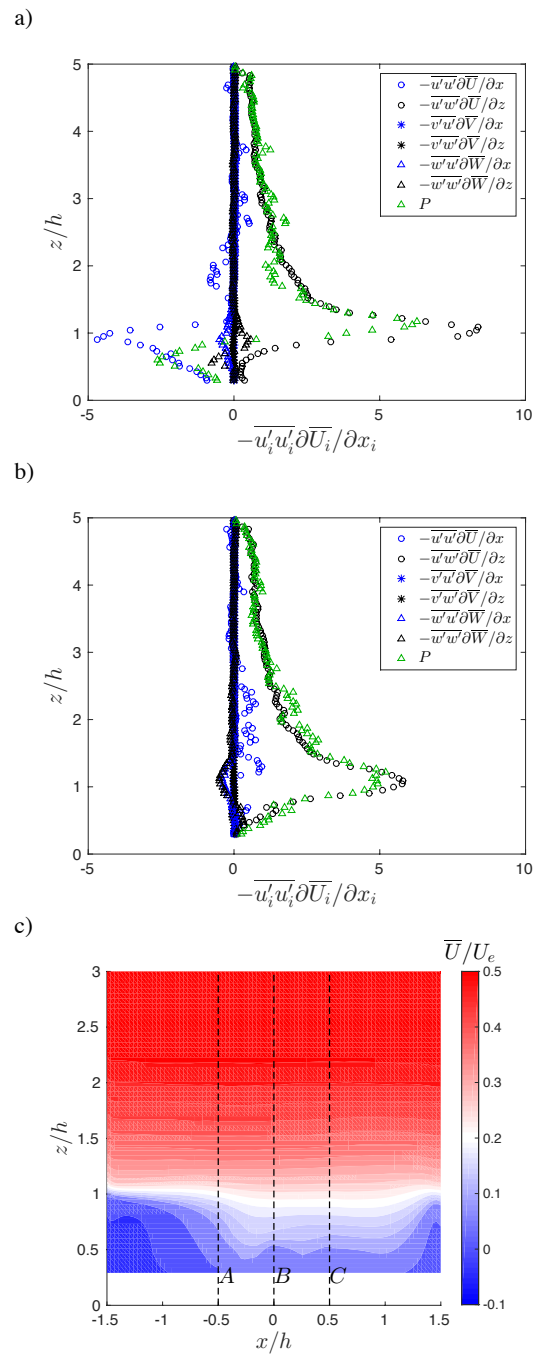
Figure 4. Decomposed turbulent production with total production (Δ) at a) A; b) B and all terms normalized by h/u_*^3; c) Mean streamwise velocity normalized by U_e.
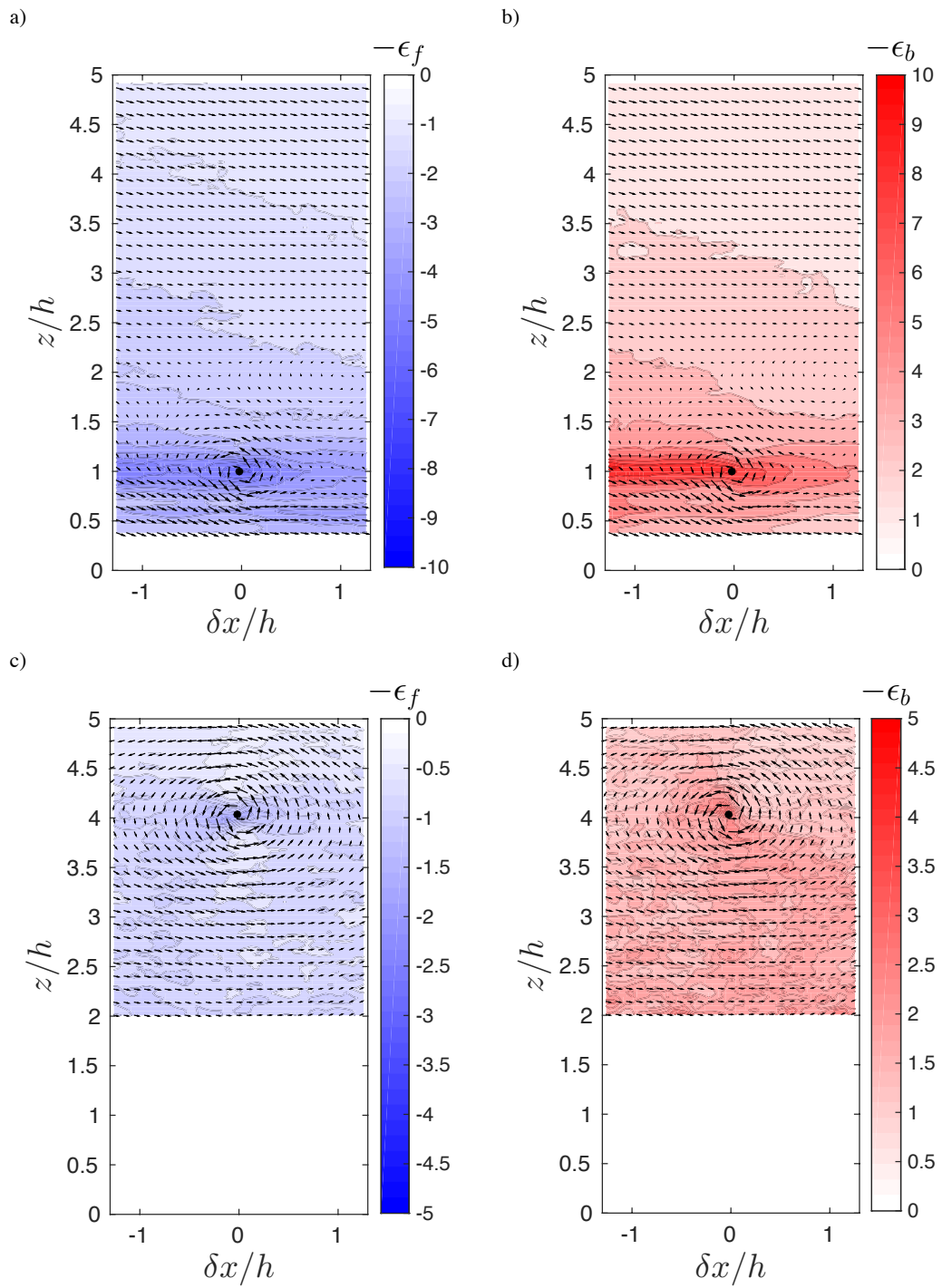
Figure 5. Conditional average of dissipation a) forward scatter and b) backscatter based on swirling event at z/h = 1 and x/h = 0; c) forward scatter and d) backscatter based on swirling event at z/h = 4 and x/h = 0.